Pergamon

Geochimica et Cosmochimica Acta, Vol. 68, No. 21, pp. 4335–4345, 2004

0016-7037/04 $30.00 + .00

doi:10.1016/j.gca.2004.01.018

Rising methane gas bubbles form massive hydrate layers at the seafloor

MATTHIAS HAECKEL,* ERWIN SUESS, KLAUS WALLMANN, and DIRK RICKERT†
GEOMAR—Research Center for Marine Geosciences, Wischhofstr. 1-3, D-24148 Kiel, Germany

(*Received June* 23, 2003; *accepted in revised form January* 23, 2004)

Abstract—Extensive methane hydrate layers are formed in the near-surface sediments of the Cascadia margin. An undissociated section of such a layer was recovered at the base of a gravity core (i.e. at a sediment depth of 120 cm) at the southern summit of Hydrate Ridge. As a result of salt exclusion during methane hydrate formation, the associated pore waters show a highly elevated chloride concentration of 809 mM. In comparison, the average background value is 543 mM.

A simple transport-reaction model was developed to reproduce the Cl^- observations and quantify processes such as hydrate formation, methane demand, and fluid flow. From this first field observation of a positive Cl^- anomaly, high hydrate formation rates (0.15–1.08 mol cm^{-2} a^{-1}) were calculated. Our model results also suggest that the fluid flow rate at the Cascadia accretionary margin is constrained to 45–300 cm a^{-1}. The amount of methane needed to build up enough methane hydrate to produce the observed chloride enrichment exceeds the methane solubility in pore water. Thus, most of the gas hydrate was most likely formed from ascending methane gas bubbles rather than solely from CH_4 dissolved in the pore water.

1. INTRODUCTION

Gas hydrates or clathrates are solid compounds with a non-stoichiometric crystalline structure hosting low molecular weight gases, such as CH_4 and H_2S, within cages formed by water molecules. Marine hydrates are common in sediments of high latitude continental shelves and the slope and rise of continental margins with organic-rich sediments (Kvenvolden, 1988, 1998). Usually, they occur at depths well below the sediment surface because methane is rapidly oxidized by microbial consortia in the shallow subsurface utilizing pore water sulfate as oxidizing agent (Boetius et al., 2000). However, clathrates are being discovered with increasing frequency in near-surface sediments at continental margin sites, where methane is rapidly transported to the seafloor by gas, mud, or fluid expulsion (Egorov et al., 1999; Ginsburg et al., 1999; Sassen et al., 2001; Suess et al., 1999).

In these areas, a high supply of methane from the subsurface exceeds the loss of methane from oxidation. These near-surface hydrate deposits are unstable due to the ongoing oxidation and dissociation and quickly vanish after the methane reservoir is exhausted at depth or the conduits for methane transport are clogged (Egorov et al., 1999). The formation mechanisms of seafloor hydrates, however, are unclear.

The Hydrate Ridge (Fig. 1) is an accretionary ridge of the Cascadia subduction zone off Oregon, where the oceanic Juan de Fuca plate is subducted beneath the continental North American plate. This tectonically active margin is composed of folded thrust slices of Pliocene-Pleistocene age. It is the second of a series of seaward-verging ridges parallel to the deformation front.

Hydrate Ridge has been the target of the Ocean Drilling Program, Leg 146 (Westbrook et al., 1994), and more recently Leg 204 (Bohrmann et al., 2002), thus underlying the importance of this area for gas hydrate research. In fact, more than a decade of research led to the documentation of active venting of fluids and gases and exposures of methane hydrates at the seafloor of Hydrate Ridge (Suess et al., 1985; Kulm et al., 1986; Suess and Whiticar, 1989; Linke et al., 1994; Bohrmann et al., 1998; Suess et al., 1999; Tryon et al., 1999; Suess et al., 2001).

The crest of Hydrate Ridge harbors seafloor hydrates and numerous vents where gas bubbles and fluids are released into the water column (Fig. 2; Suess et al., 1999, 2001). During the TECFLUX campaign (Bohrmann et al., 2000; Linke and Suess, 2001) ten sediment cores containing gas hydrate layers of various thicknesses and random intervals down to a depth of ~200 cmbsf were taken at the ridge crest. One of these cores, which is presented in this paper, terminated in a massive hydrate layer at 120 cmbsf. A thick undisturbed piece of gas hydrate (~10 cm thick) was retrieved (Fig. 3). This layer appears to extend laterally as it was encountered repeatedly over the southern summit of Hydrate Ridge. The pore waters immediately above were strongly enriched in chloride and total salt (Fig. 4). In addition, a seismic survey of the southern summit of Hydrate Ridge revealed an area of high-frequency seafloor reflectivity below the summit that covers ~400 × 600 m^2 and extends to 30 mbsf (Bohrmann et al., 2002; Trehu et al., 2002). This high reflectivity coincides with gas hydrate deposits at the seafloor and an acoustic bubble plume in the water column. Based on this reflectivity and our findings of both positive Cl^- anomalies and massive gas hydrates, cores were drilled on ODP Leg 204, Sites 1249 and 1250. They showed Cl^- enrichments of up to 1200 mM (Bohrmann et al., 2002). This confirms that our observations are representative of the southern summit of Hydrate Ridge.

In the past years, several numerical models were developed to simulate gas hydrate formation in marine sediments. They

* Author to whom correspondence should be addressed, at Dalhousie University, Department of Oceanography, 1355 Oxford Street, Halifax, NS B3H 4J1, Canada (Matthias.Haeckel@dal.ca).
† *Present address:* OMG AG & Co. KG, PC-P-AL, Rodenbacher Chaussee 4, D-63457 Hanau-Wolfgang, Germany.

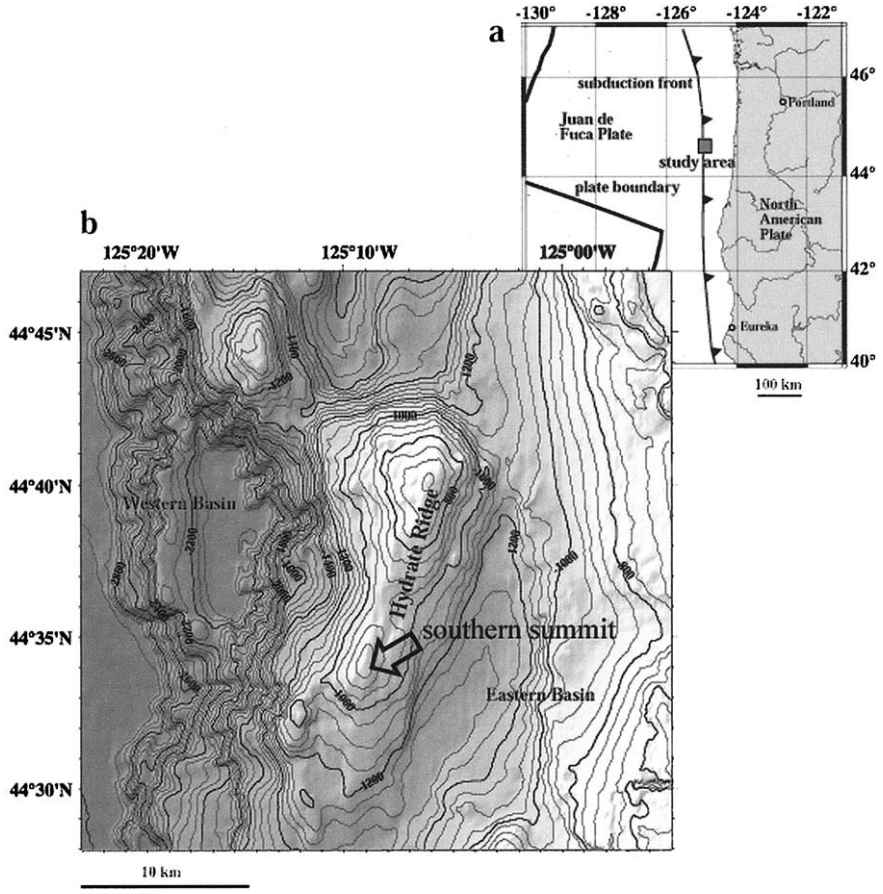

Fig. 1. Investigation area "Southern summit" of Hydrate Ridge off the coast of Oregon, WA, USA.

generally predict the average hydrate distribution in the sediment pore volume within the stability zone. These models also estimate the methane flux (Rempel and Buffett, 1997; Xu and Ruppel, 1999) as well as the associated salt exclusion (Egeberg and Dickens, 1999; Davie and Buffett, 2001). The latter is

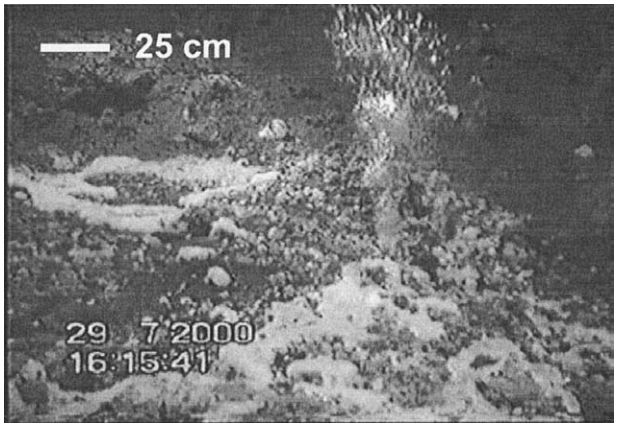

Fig. 2. Photo of cold vent site at the southern summit of Hydrate Ridge. Methane gas bubbles are ejected out of the sediment. Beggiatoa mats (white patches) mark the close surroundings of these channels for focused fluid outflow.

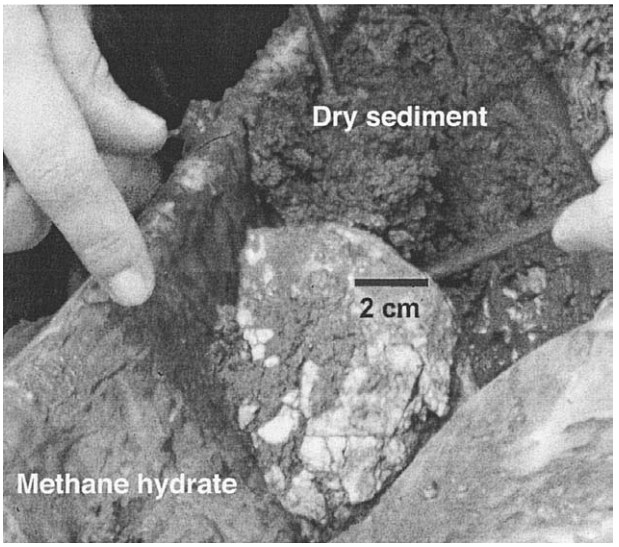

Fig. 3. Photo of the undissociated piece of methane hydrate at the bottom of core 55-5-SL, associated with the positive chloride anomaly (Figs. 4 and 5). Note the adjacent dry sediment indicating good preservation of this hydrate piece during core recovery. The gravity core did not penetrate the hydrate layer completely. It only recovered a piece from its surface.

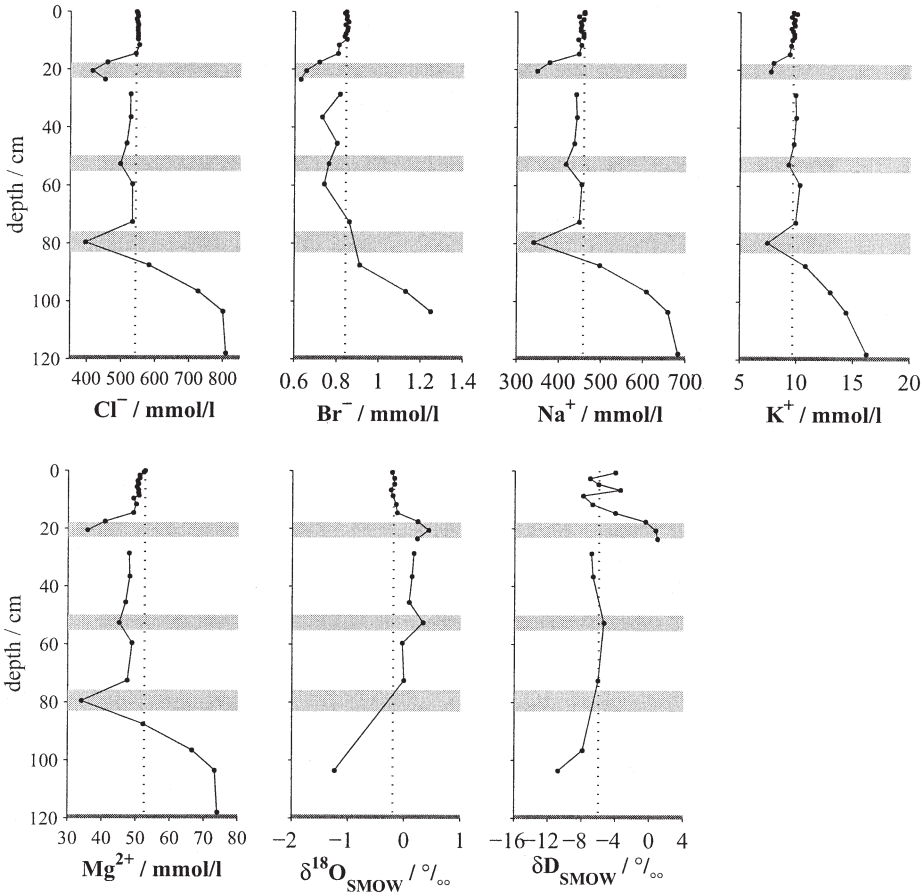

Fig. 4. Measured pore water constituents and isotopic composition (0-23 cm: 55-2C-TVMC; 26-120 cm: 55-5-SL). Lower than seawater concentrations (dotted line) are artifacts from gas hydrate dissociation (light gray areas) during core recovery (negative salt anomalies), while salt enrichments reflect active hydrate formation at the base of the core (dark gray). Isotopic ratios are above seawater level for dissociated hydrates and lower for active hydrate formation.

presented as ex situ negative chloride anomaly. We will present a model describing the formation of a discrete methane hydrate layer near the sediment surface. We simulate the observed in situ positive chloride anomaly associated with this hydrate layer and calculate its thickness and methane demand.

Here, we present data of elevated concentrations of dissolved chloride in pore waters associated with near-surface gas hydrates at Hydrate Ridge. A simple transport-reaction model reveals that these hydrates have been built from rising gas bubbles at a rate orders of magnitude faster than previously described at other locations, thus suggesting that formation is a transient process.

2. MATERIALS AND METHODS

2.1. Pore Water Analytics

During the RV SONNE expedition SO143 of July 1996 sediments were taken with a gravity corer and a multi-corer on the crest of Hydrate Ridge at a water depth of 786 m (stations 55-5-SL and 55-2C-TVMC, 44°34.210′ N, 125°08.809′ W). Pore waters were separated by squeezing of wet sediment samples, and concentrations of interstitial solutes were determined by standard analytical procedures (Grasshoff et al., 1999), i.e., Cl^- by Mohr titration, SO_4^{2-} and Br^- by ion chromatography (Sykam), Na^+, K^+, and Mg^{2+} by ICP-AES (JY 170 ULTRACE), (for further details see also: http://www.geomar.de/zd/labs/labore_umwelt/Meth_englisch.html). Pore water samples were also analyzed for isotope composition ($\delta^{18}O$ and δD) with respect to the SMOW standard using a mass spectrometer (Finnigan MAT 251). Methane concentrations were measured using the head space technique: 5 mL of sediment were placed in a 20 mL glass vial and heated at 60°C for 30 min. The head space methane was then extracted for analysis by a gaschromatograph with flame ionization detector (FID).

2.2. Numerical Model for Methane Hydrate Formation

A simple transport-reaction model was developed to simulate the observed Cl^- data. Three chemical species (chloride, methane, and gas hydrate) and the porosity change due to hydrate formation were considered.

2.2.1. Porosity

In early diagenetic models the porosity depth distribution, $\phi(x)$, generally does not change significantly with time, and hence, is prescribed by an empirical function fitted to the measured porosity data (Fig. 5). Gas hydrate formation reduces the porosity with time. Thus, porosity was calculated using:

$$\phi(x,t) = \phi_\infty + (\phi_0 - \phi_\infty)e^{-\beta x} + Ae^{-\left(\frac{x-x_0}{2\sigma}\right)^2} - GH(x,t) \qquad (1)$$

where ϕ_0 is the porosity at the sediment surface ($x=0$), ϕ_∞ is the porosity at infinite depth ($x=\infty$), β is the porosity attenuation coeffi-

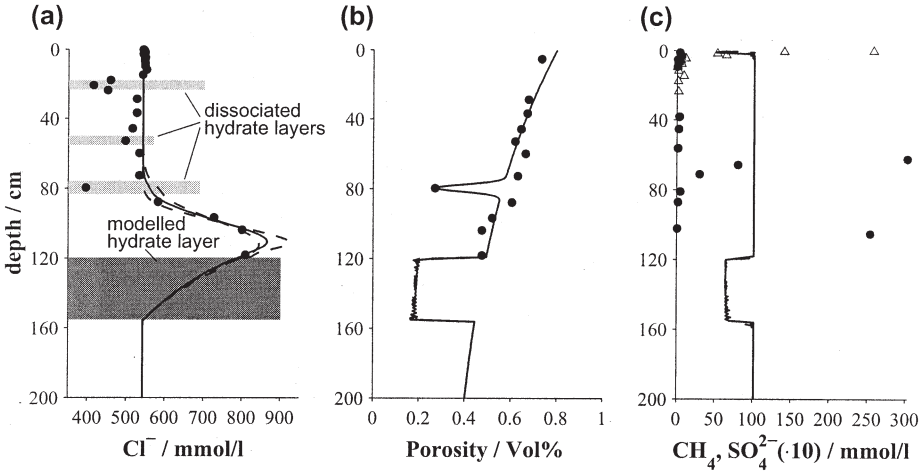

Fig. 5. (a) Measured chloride concentrations (dots) and results of least-squares fits of numerical model (solid line: t_{max} = 0.2 a; dashed lines: t_{max} = 0.07 and 0.5 a; see Table 3). The dissociated upper three hydrate layers (light gray) were not included in the fit because of their artificial Cl^- depletion. The lower massive layer (dark gray) in which the coring operation terminated is the source of the Cl^- enriched fluid. (b) Measured porosity profile (dots) and combined least-squares fit to data and model results (dashed and solid lines). The thick layer (35 cm) of low porosity represents the amount of gas hydrate necessary to produce the respective positive Cl^- anomaly (subplot a). Porosity was fitted to an empirical relationship (Eqn. 1, with $\phi_0 = 0.8$, $\phi_\infty = 0.3$, $\beta = 0.008\ cm^{-1}$, $x_0 = 79.5$ cm, A = −0.3, and $\sigma = 2$ cm). (c) Measured head space methane (dots) and sulfate (triangles) profiles and modeled methane distribution (dashed and solid lines).

cient, $Ae^{-\left(\frac{x-x_0}{2\sigma}\right)^2}$ is the porosity minimum observed at 80 cmbsf (Fig. 5b), and GH is the porosity reduction due to gas hydrate.

The 'true' porosity of hydrate-bearing, near-surface sediments results from a combination of massive hydrate pieces, gas hydrates filling pore spaces, and hydrate-free sediments. In addition, massive hydrates displace the original sediment, thus producing fractures. Despite an internal porosity close to zero, they do not seal the sediment above the hydrate layer from that below because the massive pieces are intercalated in the sediment matrix (see also Fig. 3). Our observations (Fig. 4) also clearly indicate fluid flow influence from below the hydrate layer at 120 cmbsf. This complex mechanism needs future investigation before 'true' porosity calculations are feasible. For now, we approximate the porosity reduction as if hydrate formation is solely filling the pore space. We are confident that this description leads only to small errors in our results.

2.2.2. Advection

Assuming steady state compaction, the burial velocity can be expressed as:

$$w(x,t) = \frac{1-\phi_\infty}{1-\phi(x,t)}\, w_\infty \tag{2}$$

where w_∞ = sedimentation rate at infinite depth.

Since burial and compaction at cold vent sites are much smaller than the upward fluid flow, they can be neglected and the advection rate is:

$$u(x,t) = \frac{\phi_0}{\phi(x,t)}\, u_0 \tag{3}$$

where u_0 = fluid flow rate at the sediment surface.

For fluid flow through porous media, lateral hydrodynamic dispersion coefficients, $D_L = D_S + \alpha u$, must be considered. It includes the effects of molecular diffusion (D_S) and fluid flow (αu, the product of dispersivity, α, and advection rate, u) (Appelo and Postma, 1992). However, due to the slow fluid flow rate and the fine-grained texture of sediments at cold vent sites, the solute dispersion is dominated by molecular diffusion and hence, αu can be neglected (Wallmann et al., 1997), such that $D_L = D_S$.

2.2.3. Methane hydrate formation

Methane hydrate formation is assumed proportional to the saturation state of methane in the pore water with respect to its equilibrium concentration in the presence of the hydrate phase (L_{GH}):

$$R_{GH} = k_{GH}\left(\frac{CH_4}{L_{GH}} - 1\right) \tag{4}$$

L_{GH} was calculated. The kinetic constant k_{GH} has units of volume hydrate by bulk sediment volume and time. Only the hydrate formation below 120 cmbsf is modelled, as the sediments above did not show any sign of active hydrate formation, i.e., $k_{GH} = 0$ for $x < 120$ cm (see section 3.3 for details).

Since hydrate formation withdraws methane from the pore water, the rate of methane consumption (in units of mole CH_4 per volume pore water and time) is related to R_{GH} by:

$$R_M = \frac{\rho_{GH}}{M_{GH}\phi}\, R_{GH} \tag{5}$$

where ρ_{GH} = density of methane hydrate and M_{GH} = molar weight of natural gas hydrate.

2.2.4. Methane gas dissolution

As gas bubbles rise through the sediments they are replenishing the pore water methane content. A first order rate accounts for this dissolution of ascending gas bubbles:

$$R_{MB} = k_{MB}(L_{MB} - CH_4) \tag{6}$$

where methane concentration in equilibrium with the gas phase, L_{MB}, is calculated following Foffonoff and Millard (1983) and Poisson et al. (1991).

Methane gas is represented by a source term for methane dissolved in the pore water (Eqns. 6 and 13). It is not transported explicitly by the model.

L_{GH} and L_{MB} are kept constant during the model runs because the imposed salinity change does not alter the methane equilibrium concentrations (Table 1) significantly enough to affect the model results.

Table 1. Parameters and boundary conditions used in the numerical model.[e]

Parameter	Value
Maximum depth of calculation	300 cm
Temperature	4.2°C
Pressure	78.6 atm
Salinity	34.3
w_∞ (Sedimentation rate)	0.002 cm/a[a]
$[Cl^-](x = 0,t)$	543 mmol/L
$[CH_4](x = 0,t)$	0 mmol/L
$GH(x = 0,t)$	0 vol%
$[Cl^-](x = 300cm,t)$	543 mmol/L
$[CH_4](x = 300cm,t)$	L_{MB}
$dGH/dx\|_{x = 300cm,t}$	0
L_{GH} (CH_4 equilibrium conc. with GH phase)	65 mmol/L[b]
L_{MB} (CH_4 equilibrium conc. with gas phase)	102 mmol/L[ce]
M_{GH} (molar weight of natural GH)	122.3 g/mol[d]
ρ_{GH} (GH density)	0.9 g/cm^3[d]
ρ_{PW} (pore water density)	1.035 g/cm^3[bc]

[a] Su et al. (2003)
[b] Mean value for salinity range from 34.4–50 (i.e., $[Cl^-]$ = 543–809 mM): L_{GH} = 107–97 mM, L_{MB} = 66–63 mM, ρ_{PW} = 1.031–1.039 g/cm^3.
[c] Duan et al. (1992a,b).
[d] Ussler and Paull (2001).
[e] Foffonoff and Millard (1983); Poisson et al. (1991).

Additionally, pressure and temperature stay almost constant in the investigated sediment interval.

Finally, based on (i) a persistent acoustic bubble plume in the water column above the southern summit, (ii) ROV observations of vigorous ebullition of methane gas bubbles at the seafloor (Fig. 2), and (iii) methane concentrations exceeding its solubility in pore water (Fig. 5c; observations from ODP Leg 204; Milkov et al., 2003), we believe that the assumption of an inexhaustible methane gas source is justified.

2.2.5. Chloride exclusion

During methane hydrate formation chloride is excluded from the hydrate phase and added to the surrounding pore water. This mass change of pore water over time can be expressed as:

$$m^f_{PW} = m^i_{PW} - dm_{GH} \tag{7}$$

where the indices i and f denote the mass of pore water before and after hydrate formation and dm_{GH} is the mass of the precipitated gas hydrate. Converting mass into a volume balance leads to:

$$V^f_{PW} = V^i_{PW} - \frac{\rho_{GH}}{\rho_{PW}} dV_{GH} \tag{8}$$

Thus, the change in chloride concentration, dCl, can be written:

$$dCl = Cl^f - Cl^i = \frac{n^f_{Cl}}{V^i_{PW} - \frac{\rho_{GH}}{\rho_{PW}} dV_{GH}} - Cl^i = \frac{n^i_{Cl}}{V^i_{PW} - \frac{\rho_{GH}}{\rho_{PW}} dV_{GH}} - Cl^i \tag{9}$$

where n_{Cl} = amount of chloride before (i) and after (f) hydrate formation, and $n^f_{Cl} = n^i_{Cl}$, since the total mass of chloride remains constant during hydrate formation. Rearranging gives:

$$dCl = \frac{Cl^i \rho_{GH} dV_{GH}}{\rho_{PW} V^i_{PW} - \rho_{GH} dV_{GH}} = \frac{Cl^i \rho_{GH} dGH}{\rho_{PW} \phi^i - \rho_{GH} dGH} \tag{10}$$

where porosity $\phi = V_{PW}/V_{bulkSed}$ and $dGH = dV_{GH}/V_{bulkSed}$ is porosity change due to methane hydrate formation. The rate of chloride exclusion ($R_{Cl} = dCl/dt$) is related to the hydrate formation rate ($R_{GH} = dGH/dt$) by:

$$R_{Cl} = \frac{dCl}{dt} = \frac{Cl \rho_{GH}}{\rho_{PW}\phi - \rho_{GH} dGH} R_{GH} \approx Cl \frac{\rho_{GH}}{\rho_{PW}\phi} R_{GH} \tag{11}$$

where the simplification holds when $\rho_{GH}\, dGH \ll \rho_{PW}\, \phi$ for small dt.

2.2.6. Model equations

The model's governing transport-reaction equations are

Chloride:

$$\frac{\partial \phi Cl}{\partial t} = \frac{\partial}{\partial x}\left(\phi \frac{D_{Cl}}{\theta^2}\frac{\partial Cl}{\partial x} + \phi_0 u_0 Cl\right) + Cl \frac{\rho_{GH}}{\rho_{PW}} k_{GH}\left(\frac{CH_4}{L_{GH}} - 1\right) \tag{12}$$

Methane:

$$\frac{\partial \phi CH_4}{\partial t} = \frac{\partial}{\partial x}\left(\phi \frac{D_{CH_4}}{\theta^2}\frac{\partial CH_4}{\partial x} + \phi_0 u_0 CH_4\right) - \frac{\rho_{GH}}{M_{GH}} k_{GH}\left(\frac{CH_4}{L_{GH}} - 1\right) + \phi k_{MB}(L_{MB} - CH_4) \tag{13}$$

Gas hydrate:

$$\frac{\partial GH}{\partial t} = -\frac{1 - \phi_\infty}{1 - \phi} w_\infty \frac{\partial GH}{\partial x} + k_{GH}\left(\frac{CH_4}{L_{GH}} - 1\right) \tag{14}$$

where D_i = diffusion coefficients of Cl^- and CH_4 corrected for salinity, temperature and pressure (Hayduk and Laudie, 1974; Li and Gregory, 1974), and $\theta^2 = 1 - 2\ln\phi$ is the tortuosity correction for diffusion (Boudreau, 1997).

This set of partial differential equations was solved numerically within the MATLAB environment. The discretization of Eqns. 12 to 14 was done using finite differences and a combination of Dirichlet and Neumann boundary conditions (see Table 1 for details). The initial conditions are based on the steady state profiles of the "no gas hydrate" condition: (i) constant Cl^- concentration (543 mM), (ii) methane profile if only anoxic methane oxidation is present and in equilibrium with gas phase (102 mM), (iii) no gas hydrate (0 mM), and (iv) observed porosity profile.

The solution to the PDEs (Eqns. 12 to 14) were first computed then least-squares fitted to the measured chloride data. Three parameters are fitted: (i) the advection rate (u_0), (ii) the rate constant for hydrate formation (k_{GH}), and (iii) the rate constant for gas bubble dissolution (k_{MB}). The thickness of the hydrate layer (x_{GH}) and its age (t_{max}) were then constrained by sensitivity analysis, i.e., a range of values were assumed and their fit analyzed to deduce the most appropriate thickness and age (hence by the minimization of χ^2 (Table 3)).

3. RESULTS AND DISCUSSION

3.1. Hydrate Formation and Chloride Anomaly

Gas hydrates in the marine environment largely consist of methane and pure water. During formation, the ions of sea salt are therefore excluded and should remain in the residual pore water. Theoretical, experimental, and observational research over the past several decades have dealt with this issue, known as the "missing salt" but convincing evidence for salt exclusion has remained elusive (Suess et al., 1996; Egeberg and Dickens, 1999; Ussler and Paull, 2001). The finding of unambiguous proof of excess salt is further complicated by the sampling artifact related to gas hydrate dissociation upon pressure release which causes the liberation of hydrate water. This water is low in salinity and likely wipes out and even reverses any significant positive salt anomalies, which might have been present in situ. The current consensus is that advective and diffusive transport of salt as well as ocean salinity changes over glacial-interglacial timescales also contribute to masking this effect.

The left panel of Figure 6 is a schematic of the evolution of in situ Cl^- enrichment produced during hydrate formation. The

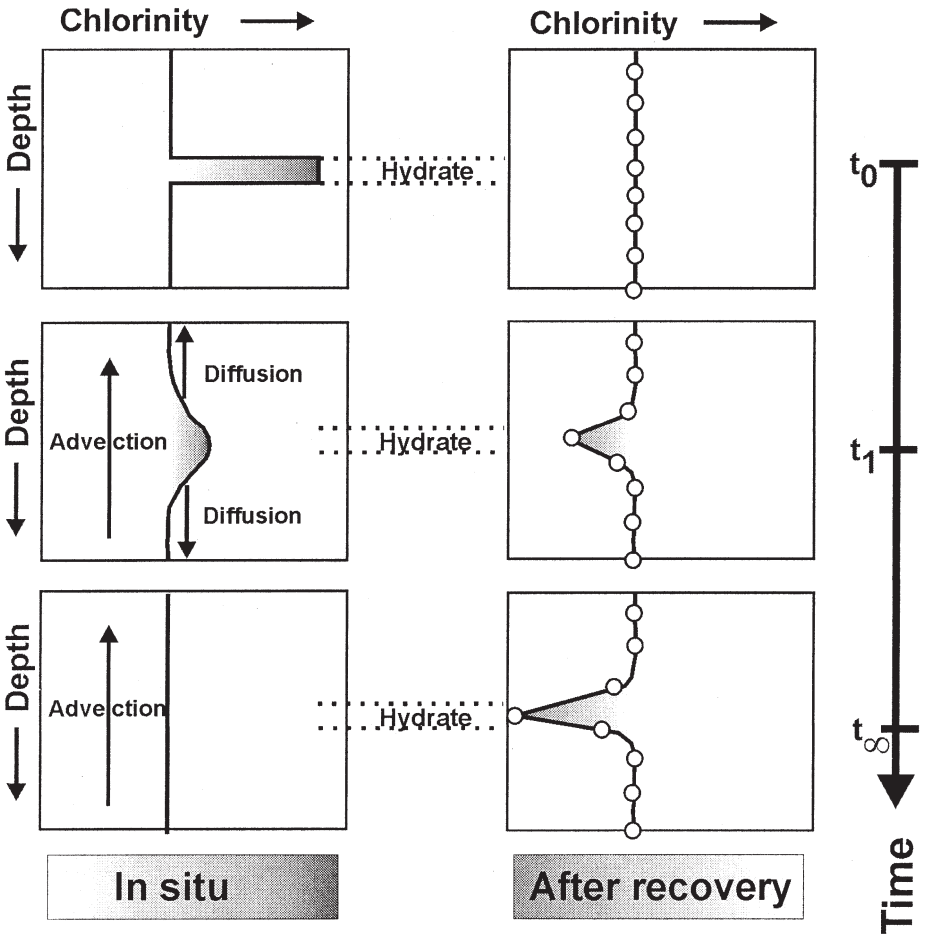

Fig. 6. Schematic evolution with time of an in situ chloride enrichment (left panel) produced by hydrate formation (t_0: active formation; t_1, t_∞: after formation has ceased) and its corresponding artificial pore water signal after recovery due to hydrate decomposition (right panel).

corresponding signal after recovery of the core is presented on the right panel. A positive in situ anomaly (time t_0, i.e., currently active formation of gas hydrate) totally vanishes during core retrieval due to hydrate decomposition. When hydrate formation ceases, the in situ Cl^- peak is weakened by advective and diffusive transport (time t_1). At this stage, pore water dilution during core retrieval alters this signal into a slightly negative Cl^- anomaly. Finally, after sufficient time (t_∞), the in situ Cl^- enrichment has vanished and hydrate dissociation during core recovery leads to a negative chloride anomaly. It is therefore at this time only that the amount of gas hydrate can be calculated correctly from the artificial ex situ measured chloride anomaly. For deep-seated hydrates (some hundreds of meters below the sediment surface), Ussler and Paull (2001) estimated the time necessary to reach t_∞ to be greater than 10,000 yr. For near-surface gas hydrates, we show that the in situ chloride peak can be leveled out within a few years depending on the depth of the hydrate layer as well as its thickness. At this shallow depth, advection might dominate over diffusion. For example, an excess Cl^- peak of ~300 mM in a sediment depth of 110 cm (similar to the one predicted from our model (Fig. 5a)), almost disappears within 1 yr if a fluid flow rate of 112 cm/a is applied (Fig. 7).

3.2. Salt Anomalies and Pore Water Isotopic Composition

Here, we present the first documentation of an extraordinary build-up of salt (Fig. 4,5a; 809 mM Cl^- versus 543 mM Cl^- in normal seawater) of pore waters adjacent to solid gas hydrate layers in near surface sediments. When quickly separating the solid hydrate from the surrounding sediment–pore water system, the release of fresh water from dissociating hydrates is sufficiently minimized ("dry sediment" in Fig. 3) to partly preserve the build-up of the excluded sea-salt concentration. Moreover, only the surface of the underlying hydrates was cored, so that the dissociation of these minor amounts could not alter the composition of the overlying pore fluids significantly.

Increasing concentrations towards the bottom of the gravity core 55-5-SL were also found for Br^-, Na^+, K^+, and Mg^{2+} (Fig. 4). These salt enrichments coincide with lower or more negative than seawater isotopic ($\delta^{18}O$ and δD) compositions of the pore water because the heavy water isotopomeres are en-

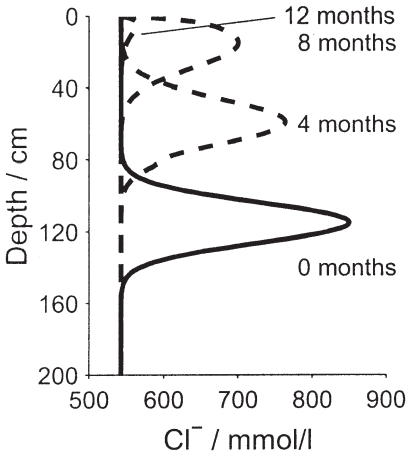

Fig. 7. Evolution of a positive Cl^- anomaly at four different times (0, 4, 8, and 12 months) after hydrate formation has ceased. Calculations are based on model results (i.e., $[Cl^-]_{max}$ = 850 mM, u_0 = 112 cm/a).

ergetically preferred in the crystal lattice during hydrate formation (Hesse and Harrison, 1981). While a single of these anomalies could be caused by other processes, e.g., magnesium release from interlayer positions in swelling clays or bromide increase from organic matter decay, the combination of the observed anomalies unambiguously points toward gas hydrate formation. Furthermore, the observation of a positive anomaly clearly indicates a currently active hydrate formation at a sediment depth of 120 cm.

Three dissociated gas hydrate layers, at 20, 55, and 80 cmbsf, were identified by their accompanied negative salt anomalies, higher than seawater isotopic composition (Fig. 4), as well as the "mousselike" sediment caused by core recovery (Westbrook et al., 1994; Kastner et al., 1995). These findings are in agreement with "old" hydrate layers where gas hydrate precipitation ceased some time ago (see section 3.1). Hence, three inactive hydrate layers were superposed above the active hydrate layer, studied here.

3.3. Model Results

Chloride concentrations show a steplike profile (Fig. 5a) indicative of rapid upward advection, from the core base, of a chloride-rich fluid. No signs of active gas hydrate precipitation were found in the sediments above the hydrate piece (Fig. 3), although the entire upper 115 m of the sediment column at the southern summit of Hydrate Ridge lie within the thermodynamic stability field (as indicated by the bottom simulating reflector; Bohrmann et al., 2002). A simple numerical diagenetic model was therefore developed and the formation of a methane hydrate layer at a sediment depth of 120 cm analyzed. The calculated chloride profiles were then least-squares fitted to the measured chloride data. Negative chloride anomalies (i.e., $[Cl^-]<530$ mM) of the dissociated "old" hydrate layers were ignored in the model though in reality the measured Cl^- gradient might be slightly steepened by the pore water freshening happening around 80 cmbsf. However, the reduced porosity due to this hydrate layer was included in the model. It did not significantly affect the model results.

Table 2. Parameter constraints from sensitivity analysis of the model.

Parameter	Value
Time of methane hydrate formation (t_{max})	0.07–0.5 a
Thickness of hydrate layer (x_{GH})	30–40 cm
Advection (fluid flow) rate (u_0)	45–300 cm/a
Rate constant for methane hydrate formation (k_{GH})	298–1022 a^{-1}
Rate constant for gas bubble dissolution (k_{MB})	459–2692 a^{-1}

The numerical model takes into account the formation of gas hydrate from dissolved methane and gas bubbles prominent in the sediments of the southern summit of Hydrate Ridge (Fig. 2). It also calculates the porosity reduction due to precipitation of hydrates in the sediment pore space and the enrichment of chloride in the remaining pore water (see section 2.2 for a detailed model description and Table 1 for input parameters).

In the model, methane consumption due to anoxic methane oxidation is handled by setting methane concentration to zero at the upper boundary. This is justified because sulfate is entirely consumed within the uppermost 3 cm of the sediments (Fig. 5c; see also Luff and Wallmann, 2003). Hence above the depth at which our first pore water sample was taken. We have tested this representation against the full description of the anoxic methane oxidation, including sulfate transport. The resulting methane profiles are graphically not distinguishable. Due to heightened cost of computation involved in using the full description, anoxic methane oxidation was handled by the surface boundary condition.

Three model parameters (u_0, k_{GH}, k_{MB}) were least-squares fitted, whereas the thickness (x_{GH}) and the age (t_{max}) of the hydrate layer were chosen to minimize χ^2 (Tables 2 and 3). Figure 5 shows (a) the results of the model fits to the chloride data, (b) the corresponding porosity profiles, and (c) the observed and calculated methane distributions. The solid line represents the best fit (t_{max} = 0.2 a), whereas the dashed lines bound the age range of t_{max} = 0.07–0.5 a within which the reproduced Cl^- peak is acceptable. Over this period a 30–40 cm gas hydrate layer is being built up (Table 2; Fig. 5b) until it fills ~30 vol% of the sediment. From these results, a depth integrated gas hydrate formation rate of 0.15–1.08 mol/(cm^2 a) is suggested.

A fluid flow rate of 45–300 cm a^{-1} was also calculated. It is constrained by the shape of the chloride profile at the core base. This rate lies within the range of values previously reported at the Cascadia convergent margin (Linke et al., 1994; Tryon et al., 1999).

To explore the linear dependence (Table 4) between the rate constants for hydrate formation, k_{GH}, and bubble dissolution, k_{MB}, on the actual hydrate formation rate, both parameters were subjected to a range of values while other parameters were kept constant (i.e., t_{max} = 0.2 a, u_0=112 cm/a, x_{GH} = 35 cm). At $k_{GH} < 2$ a^{-1} (k_{MB} = 20,000 a^{-1}) diffusion of dissolved methane is faster than consumption through hydrate formation, the methane concentrations are always higher than the theoretical methane concentration at equilibrium with the hydrate phase (L_{GH} = 65 mM). Thus, the rate of hydrate formation is dominated by its rate constant $k_{GH,}$ but hydrate formation is too slow to build up the observed chloride anomaly. At $k_{GH} > 15$ a^{-1} (k_{MB} = 899 a^{-1}) methane is consumed

Table 3. Results of least-squares fits between model and data (errors in brackets represent 95% confidence intervals).

x_{GH}/cm	t_{max}/a	u_0/cm/a	k_{GH}/a^{-1}	k_{MB}/a^{-1}	Variance	χ^2
35	0.2	112 (14)	505 (10)	899 (152)	237	1657
35	0.3	75 (13)	471 (9)	607 (181)	271	1898
35	0.4	56 (6)	366 (138)	497 (78)	426	2989
35	0.5	45 (4)	298 (21)	459 (97)	337	2365
35	0.1	236 (38)	756 (3)	1594 (328)	426	2984
35	0.07	300 (51)	1022 (87)	2692 (793)	496	3472
30	0.2	103 (12)	496 (2)	1023 (155)	313	2190
40	0.2	120 (15)	491 (6)	821 (112)	282	1973
75[a]	0.2	112 (8)	505 (33)	899 (51)	589	4126

[a] Calculation for porous methane hydrate: density $\rho_{GH} = 0.4$ g/cm^3.

by hydrate formation so fast that diffusion can no longer compensate for it (diffusion limitation). Then equilibration with the gas phase takes over as rate determining process and methane from the gas phase is immediately used for hydrate formation. In the intermediate region of $2 > k_{GH}/a < 15$, the overall hydrate formation rate is determined by both processes, hydrate formation itself and supply of methane from the gas phase.

3.4. Fluid Flow and Hydrate Formation

Figure 8 could explain the observations: methane gas bubbles and methane-saturated fluids rapidly rise to the surface entering the hydrate horizon from below. Within the hydrate layer, gas bubbles are arrested mechanically by the sediment fabric and transformed into hydrate (Ginsburg and Soloviev, 1997; Suess et al., 2001). Water is taken up in hydrates and the resulting chloride-enriched fluid is advected into the overlying sediment and mixed with the pore water.

Besides the transport of dissolved methane by fluid flow, the existence of porous gas hydrates with bubble fabric in near-surface sediments (Suess et al., 2001) suggests that gas bubbles also rise through surface sediments. This is generally believed to happen either through vent conduits (as seen in Fig. 2) or small fissures in the sediments (Sloan, 1998). Recent studies of sediments with high methane production (Martens et al., 1998; Fossing et al., 2000; Boudreau et al., 2001; Johnson et al., 2002) suggest that diffuse methane ebullition is possible when bubbles fracture the sediments due to growth and buoyancy. This transport process could explain the presence of hydrates with bubble fabric, but more research is needed before it can be described accurately. We therefore restrict our model to an inexhaustible methane source.

Our simple model, however, is well apt to assess the importance of gas bubbles in hydrate formation at Hydrate Ridge. Our results undoubtedly support gas bubbles as a major source of methane for the hydrate layer located at 120 cmbsf. This can be easily verified by omitting a methane gas source (i.e., $k_{MB} = 0$). In such case, the model predicts a Cl^- enrichment of less than 2 mM (i.e., $[Cl^-]_{max} = 545$ mM).

Table 4. Correlation matrix of fitting parameters (first fit in Table 3).

u_0	k_{GH}	k_{MB}
1	−0.8878	−0.8512
	1	0.8476
		1

Upward advection at cold vent sites is primarily driven by tectonic processes. Hyndman and Davis (1992) calculate an overall fluid flow rate of 3 mm/a for the Cascadia accretionary margin. In addition, flow rates for focused outflow at cold seeps have been measured at Hydrate Ridge (Linke et al., 1994; Tryon et al., 1999; Tryon and Brown, 2001). These authors report velocities of up to 1000 cm/a near bacterial mats decreasing to 10 cm/a in clam fields as well as variations in magnitude and direction on timescales of weeks. A simple mass balance shows that gas hydrate formation in surface sediments is likely to account, at least in part, for the high advection rates (45–300 cm/a) calculated in this study.

1 mol of natural gas hydrate consists of 1 mol of methane and 5.9 mol of water (Ussler and Paull, 2001). Hence, 1 cm^3 of methane hydrate with a density of 0.9 g/cm^3 (Ussler and Paull,

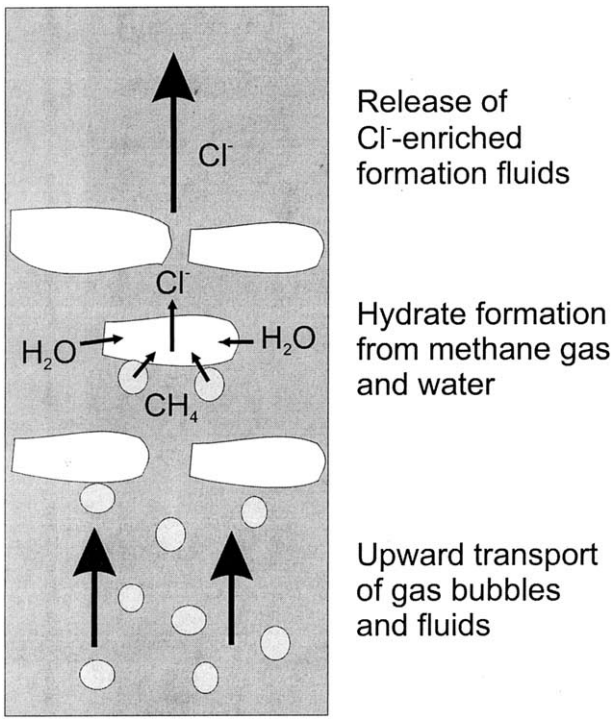

Fig. 8. Conceptual model for the formation of seafloor hydrates from rising gas bubbles and upward advecting methane-saturated fluids.

2001) contains 7.36 mmol CH_4 and 43.42 mmol H_2O. In contrast, on its formation 1 cm^3 gas hydrate replaces the same volume of water, which is equivalent to 57.5 mmol H_2O (at a salinity of 34.3, pressure of 78.6 atm, temperature of 4.2°C). Hence, 0.245 cm^3 water is displaced per cm^3 of precipitated gas hydrate. An additional volume of water is also displaced because of the density difference (~10%) itself.

In addition, 1 cm^3 of gas hydrate contains 7.357 mmol CH_4 (at a density of 0.9 g/cm^3). Following the ideal gas law, at in situ pressure and temperature this CH_4 amount occupies a volume of 2.1 cm^3. Hence, the volume is reduced by 1.1 cm^3 with respect to methane. If we include the volume difference due to water uptake and density difference, an overall volume reduction of 0.85 cm^3 results. However, for a porous hydrate fabric (at a density of 0.4 g/cm^3), the 3.27 mmol CH_4 occupy 0.94 cm^3. Therefore, the volume increases by ~0.06 cm^3 resulting in an overall volume increase of 0.72 cm^3.

Thus, a 35-cm gas hydrate layer filling up 30 vol% of the pore space over a time span of 0.2 a, will induce a fluid flow rate of 14.8 cm/a (assuming all displaced water is directed upward). If also the volume change due to gas dissolution is considered, fluid flow (−51.4 cm/a) toward the hydrate location results. If porous gas hydrates with a density of 0.4 g/cm^3, as reported for Hydrate Ridge (Suess et al., 2001), are precipitated instead, the resulting fluid flow is even higher (97.9 cm/a) and close to the value determined by the model for $t_{max} = 0.2$ a ($u_0 = 112$ cm/a; Table 3). Hence, the formation of porous hydrates might explain or contribute to the high fluid flow rates observed at Hydrate Ridge.

3.5. Quantifying Gas Bubbles

The purpose of this section is to connect the calculated gas dissolution rate, R_{MB}, to the gas bubble motion through the surface sediments. The calculations below are based on various assumptions and thus, only provide rough estimates of bubble fluxes and densities.

Gas bubbles in surface sediments have been reported to have an average radius of ~1 mm (Anderson et al., 1998). Under ambient pressure and temperature conditions (Table 1), one gas bubble contains ~14.5 μmol of methane. Hence, 1–8 bubbles/(cm^2 h) are sufficient to account for the calculated hydrate formation rate of 0.15–1.08 mol/(cm^2 a). Similarly, ~145 bubbles per cm^3 sediment are required to provide the total amount of methane stored in the modeled gas hydrate layer (~2.1 mol/L CH_4).

Boudreau et al. (2001) give the rate for the change of mass of a gas bubble (m_{MB}) when no gas source or sink is present as:

$$\frac{\partial m_{MB}}{\partial t} = 4\pi\phi R^2 D \frac{c_1 - c_0}{r} \quad (15)$$

where R = bubble radius, D = diffusion coefficient of dissolved gas, c_0 = gas concentration at bubble surface, c_1 = gas concentration at large radial distance from bubble, r = radial distance from bubble (i.e., diffusive sublayer around bubble).

This equation can be rewritten in terms of the molar gas volume, V_m, assuming a spherical gas bubble ($m_{MB}V_m = 4/3\pi R^3$):

$$\frac{\partial m_{MB}}{\partial t} = 4\pi\phi\left(\frac{3}{4\pi} m_{MB} V_m\right)^{\frac{2}{3}} D \frac{c_1 - c_0}{r} \quad (16)$$

Integrating the above equation provides a minimum estimate for bubble rise velocities in the surface sediments: assuming an average bubble radius of 1 mm at 120 cmbsf, a diffusive sublayer of 0.1 mm, a porosity of 0.6, $c_1 = L_{GH}$, and $c_0 = L_{MB}$, methane bubbles will shrink ~10% (90%) within 3 (32) min. The estimated terminal bubble rise velocity is thus 4–46 cm/min, 2–3 orders of magnitude smaller than those observed in seawater (Rehder et al., 2002).

Multiplying Eqn. 16 with the number of gas bubbles per volume sediment (z_{MB}) yields an expression that is equivalent to the rate of bubble dissolution (Eqn. 4). Comparison then gives:

$$k_{MB} = \frac{4\pi\phi R^2 D}{r} z_{MB} \quad (17)$$

Thus, the calculated values for k_{MB} (Table 2) are equivalent to having 0.2–1.3 gas bubbles permanently present per cm^3 of bulk sediment.

4. SUMMARY AND CONCLUSIONS

At the southern summit of Hydrate Ridge active methane hydrate formation in near-surface sediments was identified by a positive Cl^- anomaly and lower than seawater isotopic ($\delta^{18}O$ and δD) signatures. A numerical transport-reaction model was successfully applied to simulate the observed chloride profile. The Hydrate Ridge depth-integrated hydrate formation rate (0.15–1.08 mol cm^{-2} a^{-1}) is orders of magnitude higher than formation rates previously reported for deep-seated sedimentary hydrates (Egeberg and Dickens, 1999; Davie and Buffett, 2001). The rates are controlled by the methane supply from below which is assumed to be slow in ordinary continental margin settings but is high at vent sites where gases and fluids are focused and released from over-pressured strata through highly permeable conduits (Linke et al., 1994). Since diffusion of dissolved methane alone cannot explain the observations, the high methane demand suggests that these surface hydrates are precipitated from methane gas bubbles. The estimated rate of hydrate formation allows for the build up of a hydrate layer with a thickness of 30–40 cm within 4–10 weeks, again highlighting the dynamic nature of seafloor hydrates. These hydrate deposits are constantly dissociating at the upper surface in contact with bottom water because seawater is strongly undersaturated with respect to methane. Moreover, micro-organisms use seawater sulfate and oxygen to oxidize dissolved methane, further enhancing methane depletion at the hydrate-water interface (Boetius et al., 2000). Finally, positively buoyant gas hydrate deposits may detach from the seafloor and float as large chunk to the ocean's surface (Suess et al., 2001). The rapid formation of hydrate from rising gas bubbles has to more than compensate for these losses of methane to ocean, atmosphere, and microbial communities to maintain a build up of hydrates at the seafloor. The transient nature of the chloride profile indicates that the build up of hydrates is not continuous but episodic. Thus, the amount of hydrate at the seafloor of this active margin is probably regulated by a negative feedback

where hydrates are constantly dissociating, occasionally floated to the surface, and episodically rebuilt when tectonics reopens hydrate-clogged conduits.

Acknowledgments—The authors gratefully acknowledge the constructive comments from the editor J. J. Middelburg and three anonymous reviewers. M. Haeckel also extends his gratitude to N. Bernier for improving the style and the presentation of this manuscript. The work was supported by grants from the German Federal Ministry of Science and Technology (TECFLUX: Fkz 03G0143A and 03G0148A; OMEGA: Fkz 03G0566A). M. Haeckel was supported by the Alexander von Humboldt Foundation, Bonn. This is publication no. 4 of the GEOTECHNOLOGIEN program of BMBF and DFG.

Associate editor: J. J. Middelburg

REFERENCES

Anderson A. L., Abegg F., Hawkins J. A., Duncan M. E., and Lyons A. P. (1998) Bubble populations and acoustic interaction with the gassy floor of Eckernförde Bay. *Cont. Shelf Res.* **18,** 1807–1838.

Appelo C. A. J. and Postma D. (1992) *Geochemistry, Groundwater and Pollution*. Balkema.

Boetius A., Ravenschlag K., Schubert C. J., Rickert D., Widdel F., Gieseke A., Amann R., Jørgensen B. B., Witte U., and Pfannkuche O. (2000) A marine microbial consortium apparently mediating anaerobic oxidation of methane. *Nature* **407,** 623–626.

Bohrmann G., Greinert J., Suess E., and Torres M. (1998) Authigenic carbonates from Cascadia subduction zone and their relation to gas hydrate stability. *Geology* **26,** 647–650.

Bohrmann G., Linke P., Suess E. and Pfannkuche O. (2000) RV *Sonne* cruise report SO143. TECFLUX-I-1999, pp. 217. GEOMAR.

Bohrmann G., Trehu A. M., Rack F. R. and Shipboard Scientific Party. (2002) Leg 204 preliminary report, p. 81. Ocean Drilling Program.

Boudreau B. P. (1997) *Diagenetic Models and Their Implementation: Modelling Transport and Reactions in Aquatic Sediments*. Springer-Verlag.

Boudreau B. P., Gardiner B. S., and Johnson B. D. (2001) Rate of growth of isolated bubbles in sediments with a diagenetic source of methane. *Limnol. Oceanogr.* **46,** 616–622.

Davie M. K. and Buffett B. A. (2001) A numerical model for the formation of gas hydrate below the seafloor. *J. Geophys. Res.* **106,** 497–514.

Duan Z., Møller N., Greenberg J., and Weare J. H. (1992a) The prediction of methane solubility in natural waters to high ionic strength from 0 to 250°C and from 0 to 1600 bar. *Geochim. Cosmochim. Acta* **56,** 1451–1460.

Duan Z., Møller N., and Weare J. H. (1992b) An equation of state for the CH_4-CO_2-H_2O system: I. Pure systems from 50 to 1000°C and 0 to 8000 bar. *Geochim. Cosmochim. Acta* **56,** 2605–2617.

Egeberg P. K. and Dickens G. R. (1999) Thermodynamic and pore water halogen constraints on gas hydrate distribution at ODP Site 997 (Blake Ridge). *Chem. Geol.* **153,** 53–79.

Egorov A. V., Crane K., Vogt P. R., and Rozhov A. N. (1999) Gashydrates that outcrop on the sea floor: Stability models. *Geo-Mar. Lett.* **19,** 68–75.

Foffonoff N. P. and Millard R. C. (1983) Algorithms for computation of fundamental properties of seawater. *UNESCO Tech. Papers Mar. Sci.* **44,** 1–53.

Fossing H., Ferdelman T. G., and Berg P. (2000) Sulfate reduction and methane oxidation in continental margin sediments influenced by irrigation (South-East Atlantic off Namibia). *Geochim. Cosmochim. Acta* **64,** 897–910.

Ginsburg G. D. and Soloviev V. A. (1997) Methane migration within the submarine gas-hydrate stability zone under deep-water conditions. *Mar. Geol.* **137,** 49–57.

Ginsburg G. D., Milkov A. V., Soloviev V. A., Egorov A. V., Cherkashev G. A., Vogt P. R., Crane K., Lorenson T. D., and Khutorskoy M. D. (1999) Gas hydrate accumulation at the Hakon Mosby Mud Volcano. *Geo-Mar. Lett.* **19,** 57–67.

Grasshoff K., Ehrhardt M., Kremling K. (1999) *Methods of Seawater Analysis*. Wiley-VCH.

Hayduk W. and Laudie H. (1974) Prediction of diffusion coefficients for nonelectrolytes in dilute aqueous solutions. *Am. Inst. Chem. Eng. J.* **20,** 611–615.

Hesse R. and Harrison W. E. (1981) Gas hydrates (clathrates) causing pore water freshening and oxygen isotope fractionation in deep-water sedimentary sections of terrigenous continental margins. *Earth Planet. Sci. Lett.* **55,** 453–462.

Hyndman R. D. and Davis E. E. (1992) A mechanism for the formation of methane hydrate and seafloor bottom-simulating reflectors by vertical fluid expulsion. *J. Geophys. Res.* **97,** 7025–7041.

Johnson B. D., Boudreau B. P., Gardiner B. S., and Maas R. (2002) Mechanical response of sediments to bubble growth. *Mar. Geol.* **187,** 347–363.

Kastner M., Kvenvolden K. A., Whiticar M. J., Camerlenghi A. and Lorenson T. D. (1995) Relation between pore fluid chemistry and gas hydrate associated with bottom-simulating reflectors at the cascadia margin, Sites 889 and 892. In *Proceedings of the Ocean Drilling Program, Scientific Results*, Vol. 146 (eds. B. Carson, R. J. Westbrook, R. J. Musgrave and E. Suess), pp. 175–187. Ocean Drilling Program.

Kulm L. D., Suess E., Moore J. C., Carson B., Lewis B. T., Ritger S. D., Kadko D. C., Thornburg T. M., Embley R. W., Rugh W. D., Massoth G. J., Langseth M. G., Cochrane G. R., and Scamman R. L. (1986) Oregon subduction zone: Venting, fauna, and carbonates. *Science* **231,** 561–566.

Kvenvolden K. A. (1988) Methane hydrates and global climate. *Global Biogeochem. Cycles* **2,** 221–229.

Kvenvolden K. A. (1998) A primer on the geological occurrence of gas hydrate. In *Gas Hydrates: Relevance to World Margin Stability and Climate Change*, Vol. 137 (eds. J.-P. Henriet and J. Mienert), pp. 9–30. Geological Society of London.

Li Y.-H. and Gregory S. (1974) Diffusion of ions in sea water and in deep-sea sediments. *Geochim. Cosmochim. Acta* **38,** 703–714.

Linke P., Suess E., Torres M., Martens V., Rugh W. D., Ziebis W., and Kulm L. D. (1994) In situ measurement of fluid flow from cold seeps at active continental margins. *Deep-Sea Res. I* **41,** 721–739.

Linke P. and Suess E. (2001) RV *Sonne* cruise report SO148. TECFLUX-II-2000, p. 122. GEOMAR.

Luff R. and Wallmann K. (2003) Fluid flow, methane fluxes, carbonate precipitation and biogeochemical turnover in gas hydrate-bearing sediments at Hydrate Ridge, Cascadia Margin: Numerical modeling and mass balances. *Geochim. Cosmochim. Acta* **67,** 3403–3421.

Martens C. S., Albert D. B., and Alperin M. J. (1998) Biogeochemical processes controlling methane in gassy coastal sediments—Part 1. A model coupling organic matter flux to gas production, oxidation and transport. *Cont. Shelf Res.* **18,** 1741–1770.

Milkov A. V., Claypool G. E., Lee Y.-J., Xu W., Dickens G. R., Borowski W. S., and ODP Leg 204 Scientific Party. (2003) In situ methane concentrations at Hydrate Ridge, offshore Oregon: New constraints on the global gas hydrate inventory from an active margin. *Geology* **31,** 833–836.

Poisson A., Gadhoumi M. H., and Morcos S. (1991) Salinity and density of seawater: Tables for high salinities (42 to 50). *UNESCO Tech. Papers Mar. Sci.* **62,** 1–85.

Rehder G., Brewer P. W., Peltzer E. T., and Friederich G. (2002) Enhanced lifetime of methane bubble streams within the deep ocean. *Geophys. Res. Lett.* **29,** 10.1029.

Rempel A. and Buffett B. A. (1997) Formation and accumulation of gas hydrate in porous media. *J. Geophys. Res.* **102,** 10151–10164.

Sassen R., Sweet S. T., Milkov A. V., DeFraitas D. A. and Kennicutt M. C. (2001) Stability of thermogenic gas hydrate in the Gulf of Mexico: Constraints on models of climate change. In *Natural Gas Hydrates—Occurrence, Distribution and Detection*, Vol. 124 (eds. W. P. Dillon and C. K. Paull), pp. 131–143. American Geophysical Union.

Sloan E. D. (1998) *Clathrate Hydrates of Natural Gases*. Marcel Dekker.

Su X., Watanabe M., Trehu A., Bohrmann G., Rack F., and Party L. S. S. (2003) Biostratigraphy of late Pliocene to Holocene sediments from southern Hydrate Ridge, ODP Leg 204. *Geophys. Res. Abstr.* **5,** 14012.

Suess E., Carson B., Ritger S. D., Moore J. C., Jones M. L., Kulm L. D.

and Cochrane G. R. (1985) Biological communities at vent sites along the subduction zone off Oregon. In *The Hydrothermal Vents of the Eastern Pacific: An Overview*, Vol. 6 (ed. M. L. Jones), pp. 475–484. Biological Society of Washington, Washington, D.C.

Suess E., Bohrmann G., Linke P., Collier R. W., and Torres M. (1996) Gas hydrates and fluid venting from Cascadia accretionary margin. *Eos* **77,** 321.

Suess E., Torres M. E., Bohrmann G., Collier R. W., Greinert J., Linke P., Rehder G., Trehu A., Wallmann K., Winckler G., and Zuleger E. (1999) Gas hydrate destabilization: Enhanced dewatering, benthic material turnover and large methane plumes at the Cascadia convergent margin. *Earth Planet. Sci. Lett.* **170,** 1–15.

Suess E., Torres M. E., Bohrmann G., Collier R. W., Rickert D., Goldfinger C., Linke P., Heuser A., Sahling H., Heeschen K., Jung C., Nakamura K., Greinert J., Pfannkuche O., Trehu A., Klinkhammer G., Whiticar M. J., Eisenhauer A., Teichert B. and Elvert M. (2001) Sea floor methane hydrates at Hydrate Ridge, Cascadia Margin. In *Natural Gas Hydrates—Occurrence, Distribution and Detection*, Vol. 124 (eds. W. P. Dillon and C. K. Paull), pp. 87–98. American Geophysical Union.

Suess E. and Whiticar M. J. (1989) Methane-derived CO_2 in pore fluids expelled from the Oregon subduction zone. *Palaeogeogr. Palaeoclimat. Palaeoecol.* **71,** 119–136.

Trehu A., Bangs N. L., Arsenault M. A., Bohrmann G., Goldfinger C., Johnson J. E., Nakamura Y., and Torres M. E. (2002) Complex subsurface plumbing beneath Southern Hydrate Ridge, Oregon continental margin, from high-resolution 3D seismic reflection and OBS data. *4th International Conference on Gas Hydrates.* Yokohama, Japan, 90–96.

Tryon M. D., Brown K. M., Torres M. E., Trehu A. M., McManus J., and Collier R. W. (1999) Measurements of transience and downward fluid flow near episodic gas vents, Hydrate Ridge, Cascadia. *Geology* **27,** 1075–1078.

Tryon M. D. and Brown K. M. (2001) Complex flow patterns through Hydrate Ridge and their impact on seep biota. *Geophys. Res. Lett.* **28,** 2863–2866.

Ussler W. and Paull C. K. (2001) Ion exclusion associated with marine gas hydrate deposits. In *Natural Gas Hydrates—Occurrence, Distribution and Detection*, Vol. 124 (eds. W. P. Dillon and C. K. Paull), pp. 41–51. American Geophysical Union.

Wallmann K., Linke P., Suess E., Bohrmann G., Sahling H., Schlüter M., Dählmann A., Lammers S., Greinert J., and Mirbach N. v. (1997) Quantifying fluid flow, solute mixing, and biogeochemical turnover at cold vents of the eastern Aleutian subduction zone. *Geochim. Cosmochim. Acta* **61,** 5209–5219.

Westbrook G. K., Carson B., Musgrave R. J., and Suess E. (1994) *Proceedings of the Ocean Drilling Program, Initial Reports* **146,** p. 477. Ocean Drilling Program.

Xu W. and Ruppel C. (1999) Predicting the occurrence, distribution, and evolution of methane gas hydrate in porous marine sediments. *J. Geophys. Res.* **104,** 5081–5095.